Supporting Information for

Large and anisotropic carrier mobility in monolayers of the MA$_2$Z$_4$ series (M=Cr, Mo, W; A=Si, Ge; Z=N, P)

Achintya Priydarshi,[1, *] Yogesh Singh Chauhan,[1, †] Somnath Bhowmick,[2, ‡] and Amit Agarwal[3, §]

[1]*Department of Electrical Engineering, Indian Institute of Technology Kanpur, Kanpur 208016, India*

[2]*Department of Materials Science and Engineering,*

Indian Institute of Technology Kanpur, Kanpur 208016, India

[3]*Department of Physics, Indian Institute of Technology Kanpur, Kanpur 208016, India*

(Dated: July 14, 2022)

[*] achintya@iitk.ac.in

[†] chauhan@iitk.ac.in

[‡] bsomnath@iitk.ac.in

[§] amitag@iitk.ac.in

I. LIST OF TABLES

TABLE S1: Structural parameters and DFT-PBE calculated electronic band gap of relaxed MA_2Z_4 monolayers.

Material	a	b	d_1	d_2	$d_{3,4}$	$\theta_{1,2}$	$\theta_{3,4}$	E_g
	(Å)	(Å)	(Å)	(Å)	(Å)	(°)	(°)	(eV)
$MoSi_2N_4$	2.90	5.03	2.90	2.09	1.75, 1.74	73.6,87.8	112.0,106.8	1.86
$MoGe_2N_4$	3.02	5.23	3.02	2.12	1.85,1.86	69.7,90.6	109.4,109.5	1.00
$MoSi_2P_4$	3.45	5.98	3.45	2.45	2.24,2.21	71.0,89.6	100.9,117.1	0.70
$MoGe_2P_4$	3.52	6.09	3.52	2.46	2.31,2.30	68.9,91.2	99.3,118.4	0.58
WSi_2N_4	2.89	5.01	2.89	2.09	1.74,1.75	73.8,87.7	111.9,106.9	2.17
WGe_2N_4	3.00	5.20	3.00	2.12	1.85,1.86	69.7,90.6	109.4,109.5	1.30
WSi_2P_4	3.47	6.01	3.47	2.45	2.24,2.21	70.0,90.3	101.3,116.8	0.48
WGe_2P_4	3.53	6.11	3.53	2.46	2.31,2.29	67.9,91.8	99.6,118.1	0.44
$CrSi_2N_4$	2.85	4.94	2.85	2.02	1.73,1.74	71.1,89.6	111.0,107.9	0.62
$CrGe_2N_4$	2.95	5.11	2.95	2.04	1.83,1.87	66.5,92.9	107.7,111.2	NA
$CrSi_2P_4$	3.41	5.91	3.41	2.37	2.22,2.22	67.6,92.0	99.9,117.8	0.30
$CrGe_2P_4$	3.47	6.01	3.47	2.38	2.30,2.31	64.9,93.9	98.3,119.1	NA

TABLE S2: A comparison of the effective mass at VBM and CBM and charge carrier mobility in materials in which the impact of SOC is not negligible. The values outside and inside the parentheses represent the quantity without and with SOC, respectively.

Material	Carrier type	m_x^*/m_0	m_y^*/m_0	μ_x	μ_y
				$(10^3\text{cm}^2\text{V}^{-1}\text{s}^{-1})$	$(10^3\text{cm}^2\text{V}^{-1}\text{s}^{-1})$
WSi$_2$P$_4$	e$_{X'}$	0.175(0.129)	0.178(0.130)	5.18(9.57)	6.42(12.01)
	h$_{X'}$	0.218(0.155)	0.225(0.155)	10.01(20.17)	7.01(14.60)
WGe$_2$P$_4$	e$_{X'}$	0.194(0.134)	0.199(0.133)	5.30(11.32)	6.97(15.38)
	h$_{X'}$	0.211(0.152)	0.301(0.223)	8.78(16.70)	5.33(9.86)

TABLE S3: The acoustic phonon limited carrier mobility for the MA_2Z_4 monolayers. Values inside and outside the parentheses correspond to the mobility calculated using equations S1 and S2, respectively.

Material	Carrier type	μ_x	μ_y
		$(10^3 cm^2 V^{-1} s^{-1})$	$(10^3 cm^2 V^{-1} s^{-1})$
$MoSi_2N_4$	$e_{X'}$	0.28(0.28)	0.27(0.28)
	h_Γ	0.39(0.37)	0.32(0.34)
	$h_{X'}$	2.29(1.99)	1.57(1.77)
$MoGe_2N_4$	$e_{X'}$	6.09(6.59)	7.68(7.00)
	h_Γ	1.52(1.55)	1.72(1.61)
	$h_{X'}$	8.43(7.53)	6.05(6.71)
$MoSi_2P_4$	$e_{X'}$	1.37(1.98)	1.57(1.81)
	h_Γ	0.47(0.45)	0.41(0.43)
	$h_{X'}$	5.01(4.51)	3.53(3.90)
$MoGe_2P_4$	$e_{X'}$	1.62(1.98)	2.92(2.29)
	h_Γ	0.33(0.28)	0.09(0.11)
	$h_{X'}$	6.42(5.86)	4.23(4.61)
WSi_2N_4	e_Γ	2.97(2.64)	1.36(1.51)
	$e_{X'}$	2.52(2.77)	3.23(2.94)
	e_S	0.68(0.68)	0.64(0.63)
	h_Γ	0.37(0.38)	0.38(0.38)
	$h_{X'}$	1.41(1.34)	1.17(1.22)
WGe_2N_4	$e_{X'}$	12.41(10.57)	7.33(8.48)
	h_Γ	1.34(1.30)	1.24(1.28)
	$h_{X'}$	2.42(2.40)	2.09(2.13)
WSi_2P_4	$e_{X'}$	5.18(5.63)	6.42(5.87)
	h_Γ	0.28(0.23)	0.20(0.24)
	$h_{X'}$	10.01(8.82)	7.01(7.89)
WGe_2P_4	$e_{X'}$	5.30(5.90)	6.97(6.20)
	h_Γ	0.35(0.36)	0.24(0.23)
	$h_{X'}$	8.78(8.32)	5.33(5.63)
$CrSi_2N_4$	$e_{X'}$	6.05(6.99)	8.99(7.60)
	h_Γ	0.39(0.36)	0.40(0.35)
	$h_{X'}$	4.32(4.16)	3.64(3.80)
$CrSi_2P_4$	$e_{X'}$	1.06(1.04)	0.96(0.98)
	h_Γ	0.40(0.47)	1.37(1.14)
	$h_{X'}$	1.43(1.63)	2.01(1.72)

TABLE S4: A comparison of band gap (eV) and charge carrier mobility (Unit:10^3 cm^{2}V^{-1}s^{-1}) in various 2D materials.

Material	E_g	μ_x^e	μ_y^e	μ_x^h	μ_y^h	ref
ZrS$_2$	1.16	0.97	0.020	0.072	0.262	[1]
ZrSe$_2$	0.38	3.92	0.022	0.12	0.59	[1]
ZrSSe	0.66	1.36	0.018	0.10	0.45	[1]
ZrSeTe	-0.04	1.15	0.005	1.21	2.23	[1]
ZrSTe	-0.12	0.91	0.001	2.80	1.46	[1]
HfS$_2$	1.33	2.55	0.003	0.067	0.49	[1]
HfSe$_2$	0.48	0.60	0.035	0.24	0.33	[1]
HfSSe$_2$	0.74	3.82	0.025	0.17	0.15	[1]
HfSeTe	-0.03	3.31	0.007	0.56	0.26	[1]
HfSTe	-0.23	1.86	0.002	0.62	0.57	[1]
Nb$_2$Se$_9$	0.83	1.91	0.03	0.029	0.027	[2]
SnSe	0.5	1.17	2.10	0.69	0.72	[3]
PC$_6$	0.84	294	3.2	24.80	164	[4]
Nb$_3$SBr$_7$	0.72	NA	NA	NA	NA	[5]
Ta$_3$SBr$_7$	0.75	NA	NA	NA	NA	[5]
MoSi$_2$N$_4$/CrCl$_3$	1.85	NA	NA	NA	NA	[6]
MoSe$_2$/MoSi$_2$N$_4$	1.38	1.84	1.85	22.35	22.69	[7]

TABLE S5: Strain-dependent effective mass and carrier mobility in $MoGe_2P_4$, WSi_2N_4 and WGe_2P_4 monolayer. Note that the carrier's mobility changes in response to uniaxial strain only when VBM or CBM is shifting.

Material	Strain (%) (CBM/VBM location)		Carrier type	m_x^*/m_0	m_x^*/m_0	E_x (eV)	E_y (eV)	C_x (J/m^2)	C_y (J/m^2)	μ_x ($10^3 cm^2 V^{-1} s^{-1}$)	μ_y ($10^3 cm^2 V^{-1} s^{-1}$)
$MoGe_2P_4$	σ_x	-3	$e_{x'}$				No change				
			$h_{x'}$								
		3	$e_{x'}$								
		VBM at Γ	$h_{x'}$	1.262	2.616	1.97	2.50	207.18	211.67	0.32	0.09
	σ_y	-3	$e_{x'}$				No change				
			$h_{x'}$								
		3	$e_{x'}$								
		VBM at Γ	$h_{x'}$	1.294	2.615	1.97	2.50	207.18	211.67	0.31	0.098
WSi_2N_4	σ_x	-3 **CBM at S**	e_s	0.624	0.556	5.33	5.88	521.26	521.70	0.69	0.64
			$h_Γ$				No change				
		3 **CBM at Γ**	$e_Γ$	0.311	0.520	4.32	5.01	521.26	521.70	2.90	1.12
			$h_Γ$				No change				
	σ_y	-3 **CBM at Γ**	$e_Γ$	0.320	0.520	4.32	5.01	521.26	521.70	2.98	1.37
			$h_Γ$				No change				
		3 **CBM at X'**	$e_{x'}$				No change				
			$h_Γ$				No change				
WGe_2P_4	σ_x	-3	$e_{x'}$				No change				
			$h_{x'}$								
		3 **VBM at Γ**	$e_{x'}$								
			$h_{x'}$	1.283	2.101	2.05	1.96	219.50	219.51	0.35	0.23
	σ_y	-3	$e_{x'}$				No change				
			$h_{x'}$								
		3 **VBM at Γ**	$e_{x'}$								
			$h_{x'}$	1.281	2.109	2.05	1.96	219.50	219.51	0.35	0.23

II. LIST OF FIGURES
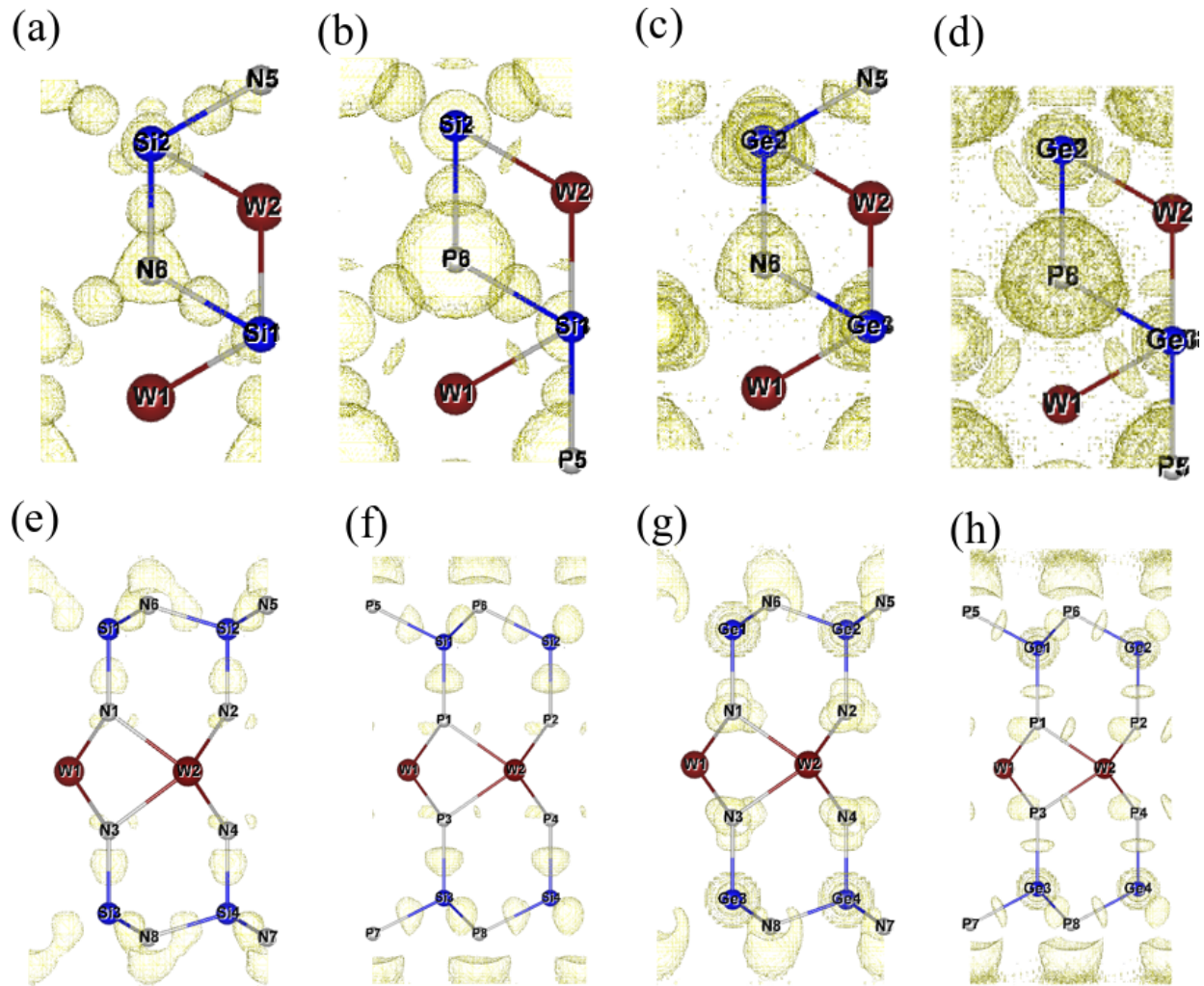
FIG. S1: (a)-(d) The top view and (e)-(f) The side of electron localization function (ELF) in WSi$_2$N$_4$, WSi$_2$P$_4$, WGe$_2$N$_4$ and WGe$_2$P$_4$ monolayers. The isosurface value is set to be 0.85 e Å^{-3}.
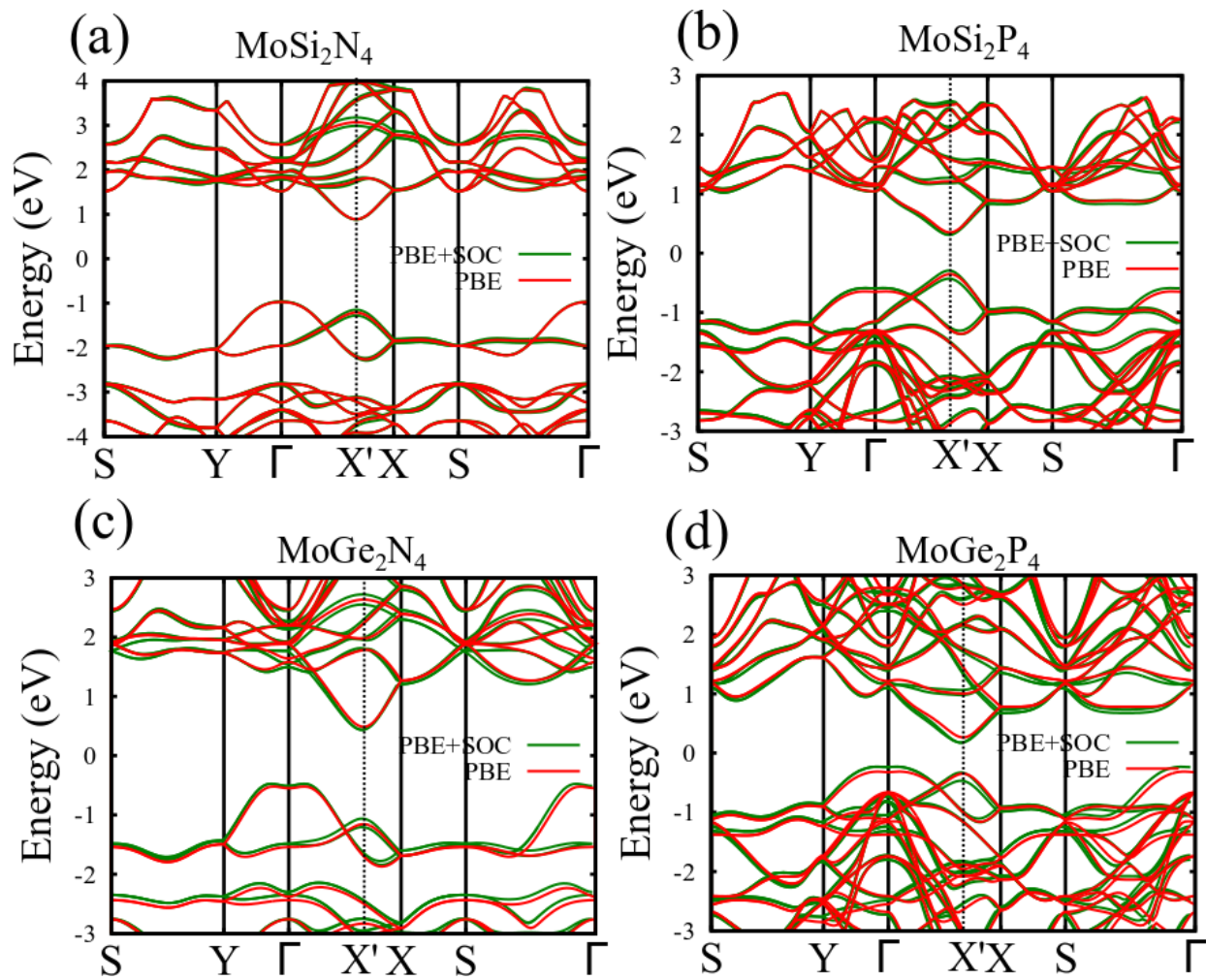
FIG. S2: PBE and PBE+SOC bandstructure of MoA_2Z_4 monolayers. The red and green lines represent PBE and PBE+SOC results, respectively.
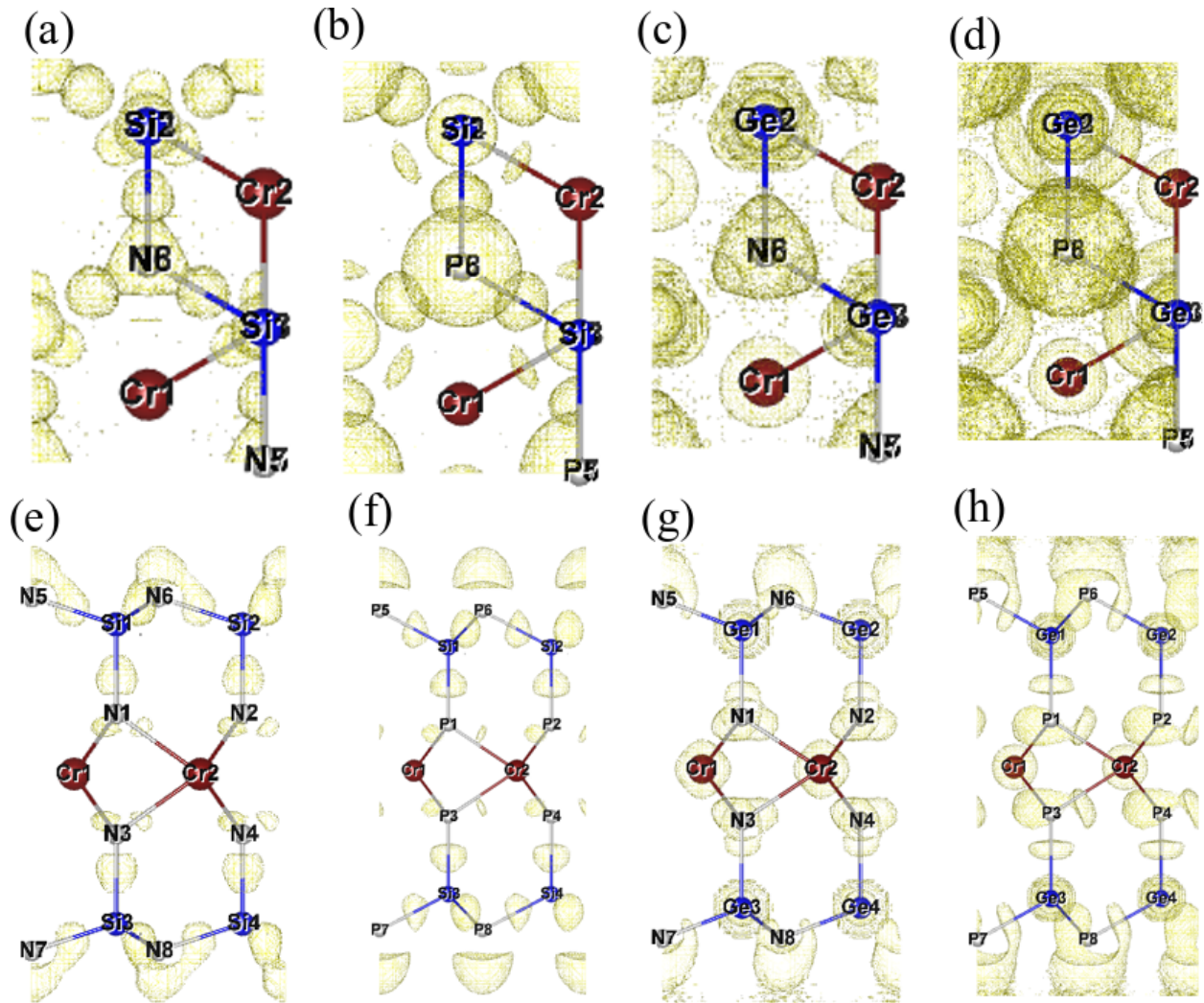
FIG. S3: (a)-(d) The top view and (e)-(f) The side of electron localization function (ELF) in CrSi$_2$N$_4$, CrSi$_2$P$_4$, CrGe$_2$N$_4$ and CrGe$_2$P$_4$ monolayers. The isosurface value is set to be 0.85 e Å^{-3}.
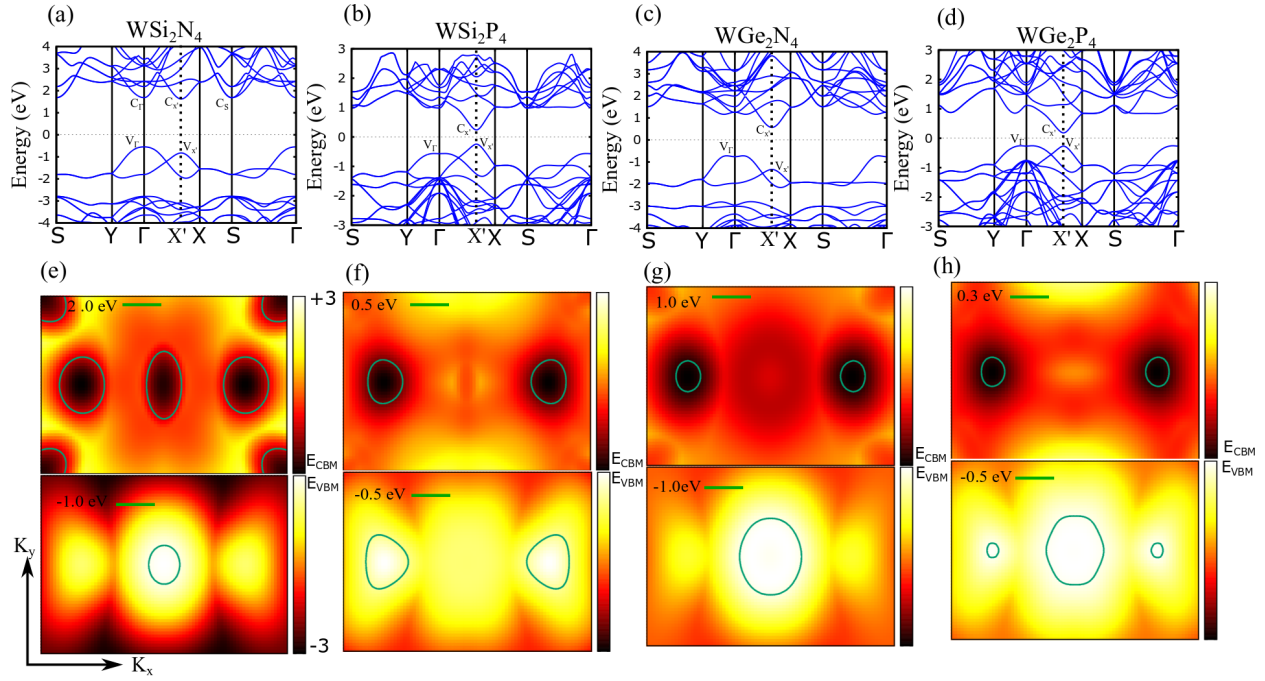
FIG. S4: The electronic band structures of (a) WSi$_2$N$_4$, (b)WSi$_2$P$_4$, (c) WGe$_2$N$_4$ and (d) WGe$_2$P$_4$ monolayers. (e)-(h) Corresponding 2D plots of the conduction (top panel) and valence band (bottom panel) energy over the entire Brillouin zone.
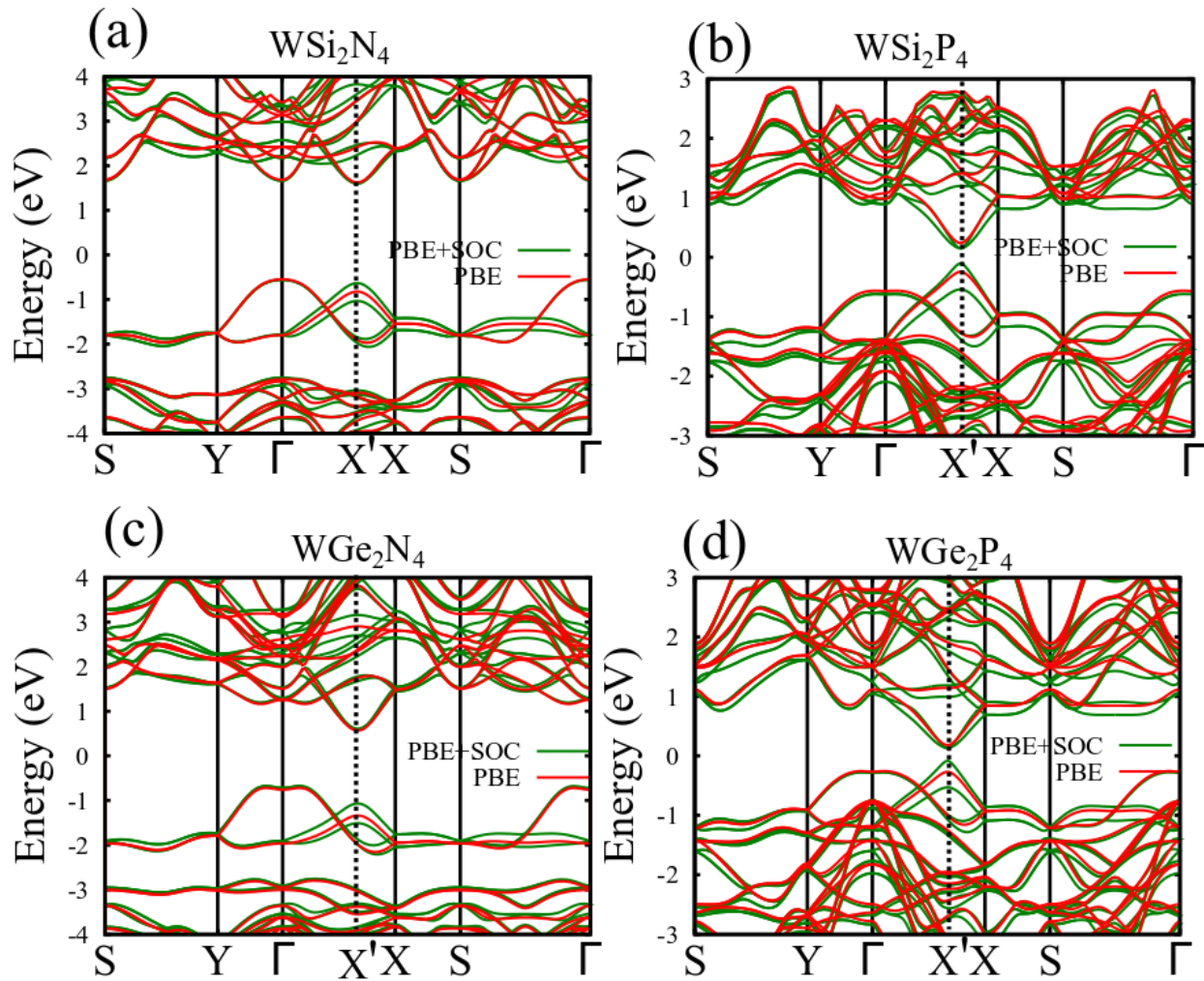
FIG. S5: PBE and PBE+SOC bandstructure of WA$_2$Z$_4$ monolayers. The red and green lines represent PBE and PBE+SOC results, respectively.
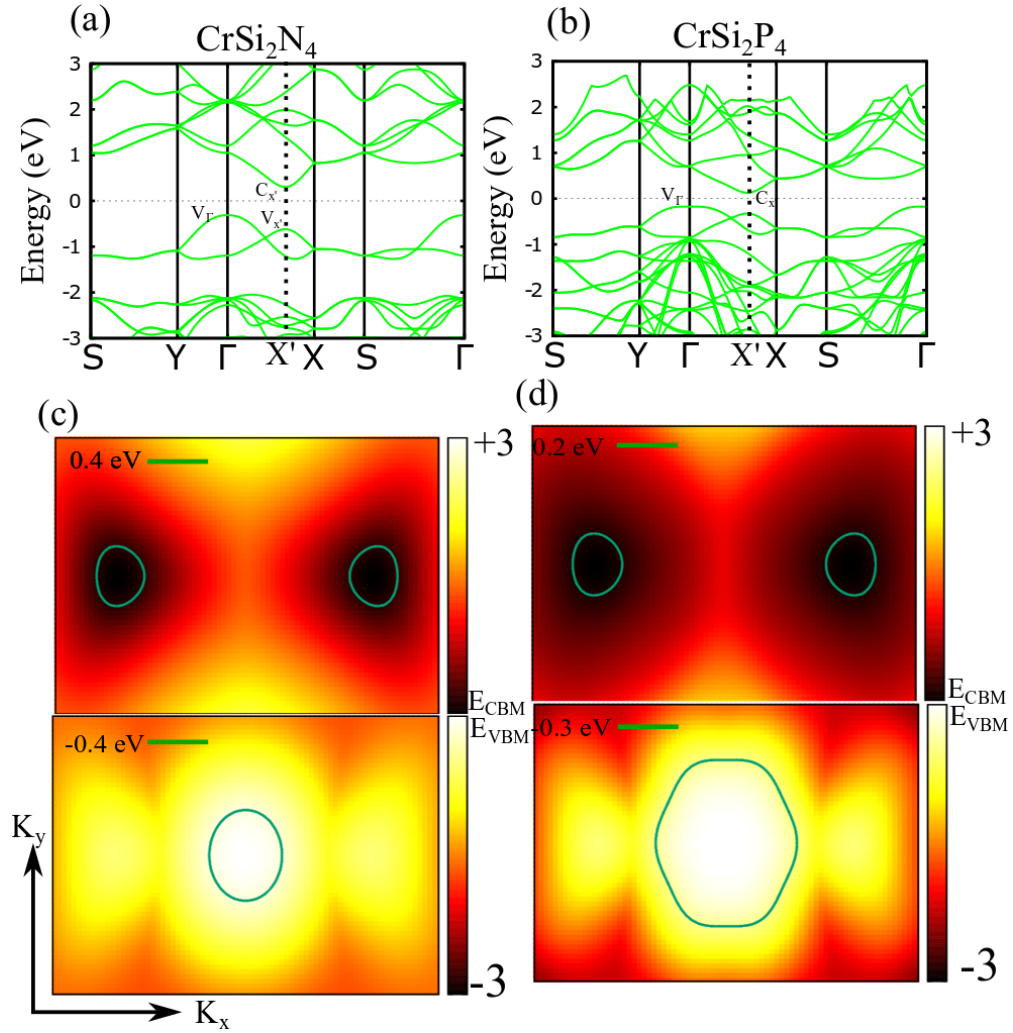
FIG. S6: (a)-(b) The electronic band structures of $CrSi_2N_4$ and $CrSi_2P_4$, (c)-(d) Corresponding 2D plots of the conduction (top panel) and valence band (bottom panel) energy over the entire Brillouin zone.
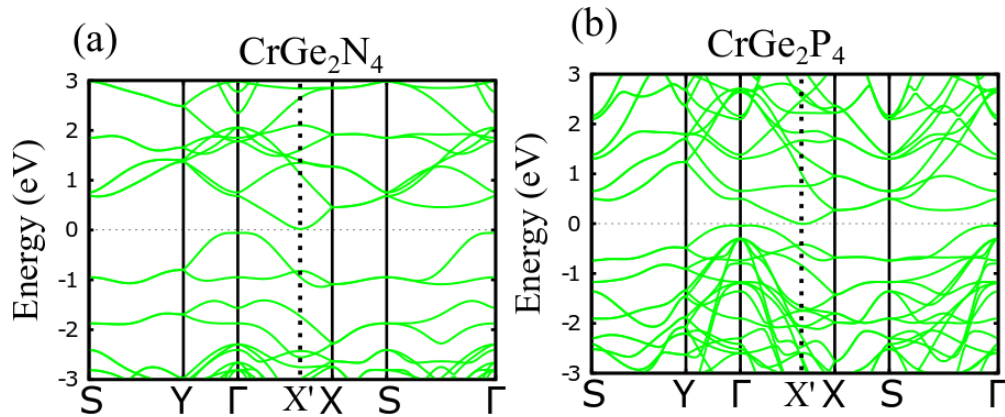
FIG. S7: The electronic band structures of (a) $CrGe_2N_4$, and (b) $CrGe_2P_4$.
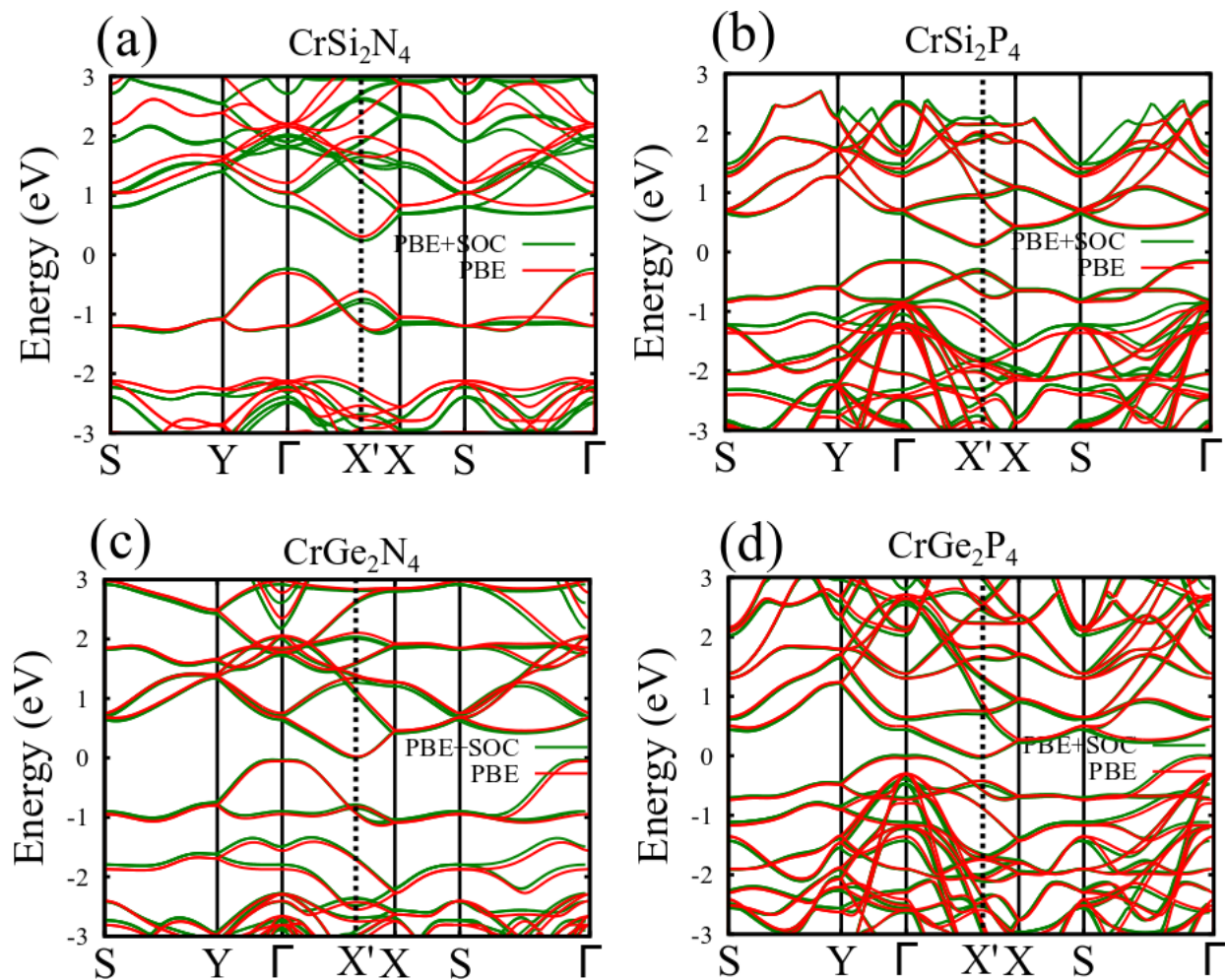
FIG. S8: PBE and PBE+SOC bandstructure of CrA$_2$Z$_4$ monolayers. The red and green lines represent PBE and PBE+SOC results, respectively.
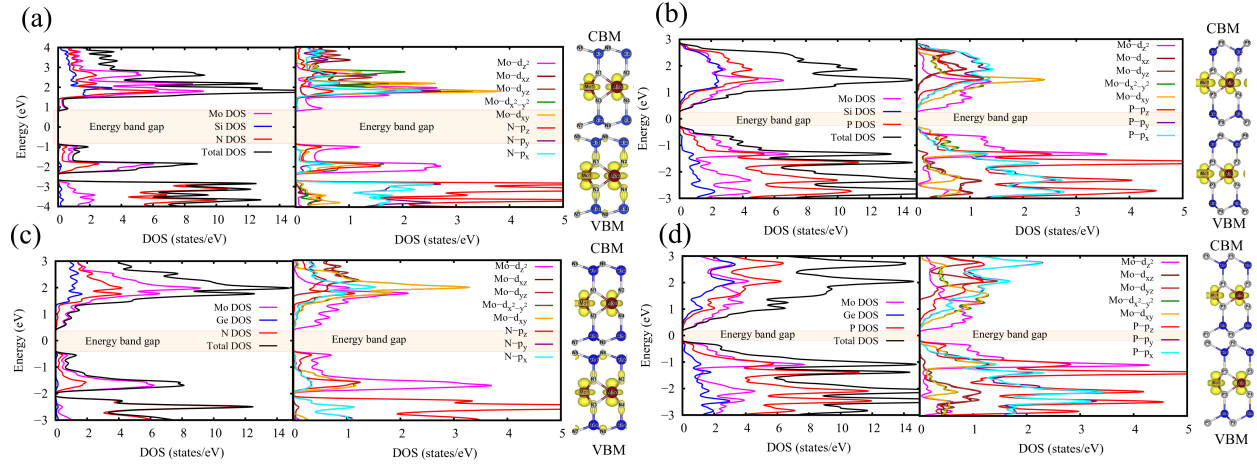
FIG. S9: The atom projected density of states of monolayer (a) $MoSi_2N_4$, (b) $MoSi_2P_4$, (c) $MoGe_2N_4$ and (d) $MoGe_2P_4$. The right panel of the figures displays the corresponding wave functions at the valence band maximum (VBM) and at the conduction band minimum (CBM). Clearly, the Mo states dominate the DOS near the electronic bandgap. The isosurface value is set to be 0.002 $e\text{Å}^{-3}$.
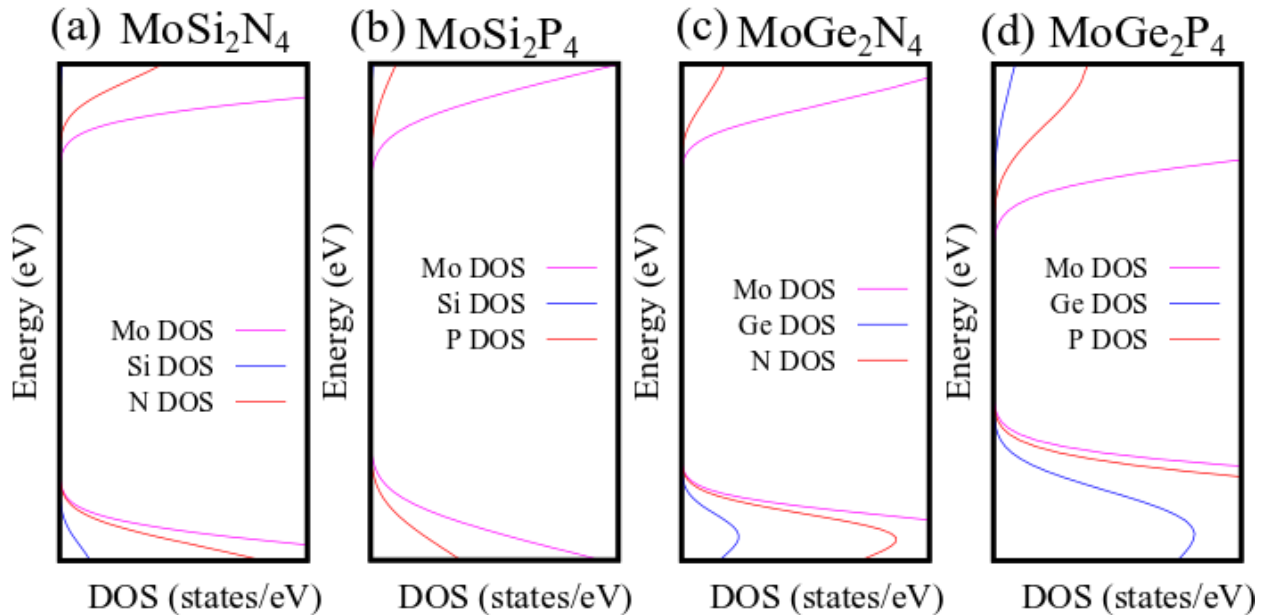

FIG. S10: A zoomed view of PDOS near VBM and CBM in MoA_2Z_4 monolayers. In VBM, the contribution from P atoms is less than that of N atoms.
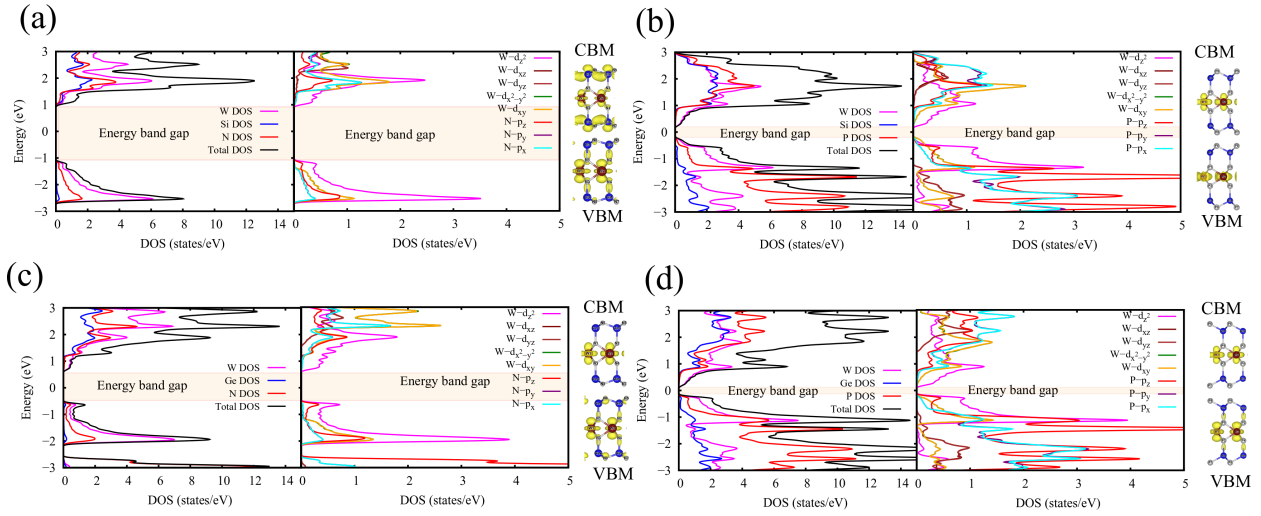
FIG. S11: The atom projected density of states of monolayer (a) WSi_2N_4, (b) WSi_2P_4, (c) WGe_2N_4 and (d) WGe_2P_4. The right panel of the figures displays the corresponding wave functions at the valence band maximum (VBM) and at the conduction band minimum (CBM). Clearly, the W states dominate the DOS near the electronic bandgap. The isosurface value is set to be 0.002 $e\text{Å}^{-3}$.
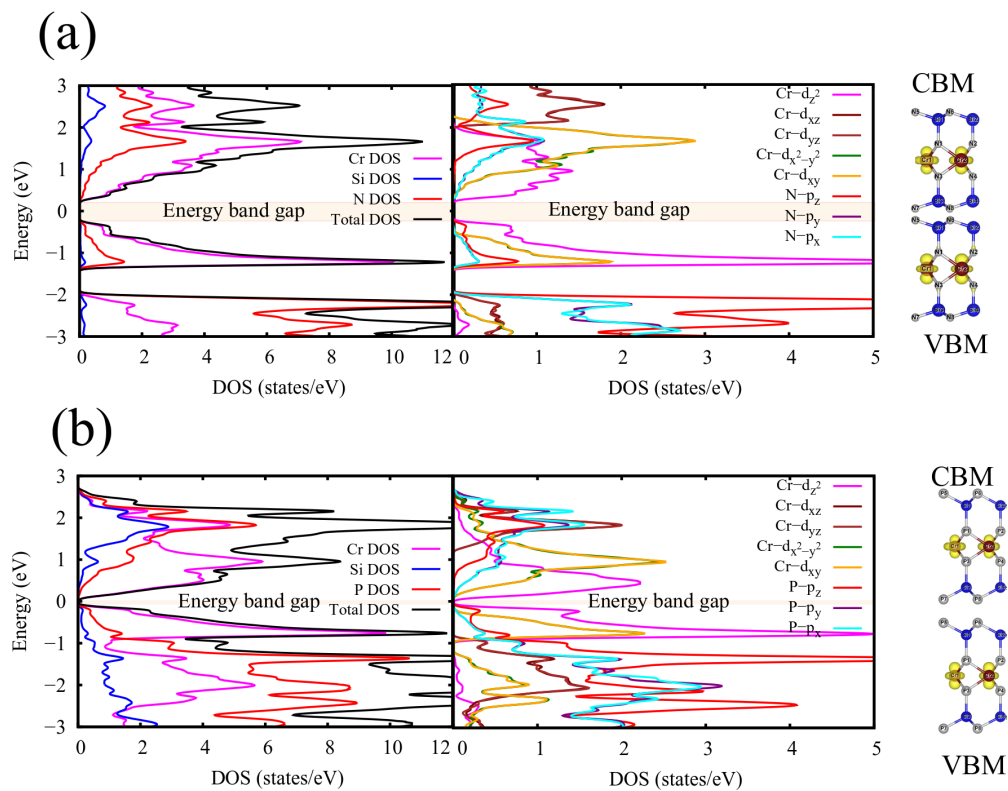
FIG. S12: The atom projected density of states of monolayer (a) CrSi$_2$N$_4$ and (b) CrSi$_2$P$_4$. The right panel of the figures displays the corresponding wave functions at the valence band maximum (VBM) and at the conduction band minimum (CBM). Clearly, the Cr states dominate the DOS near the electronic bandgap. The isosurface value is set to be 0.002 eÅ^{-3}.
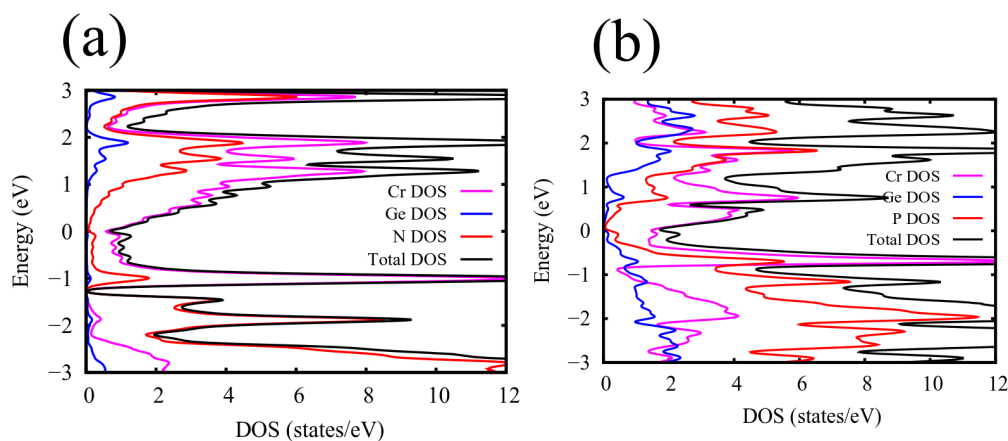
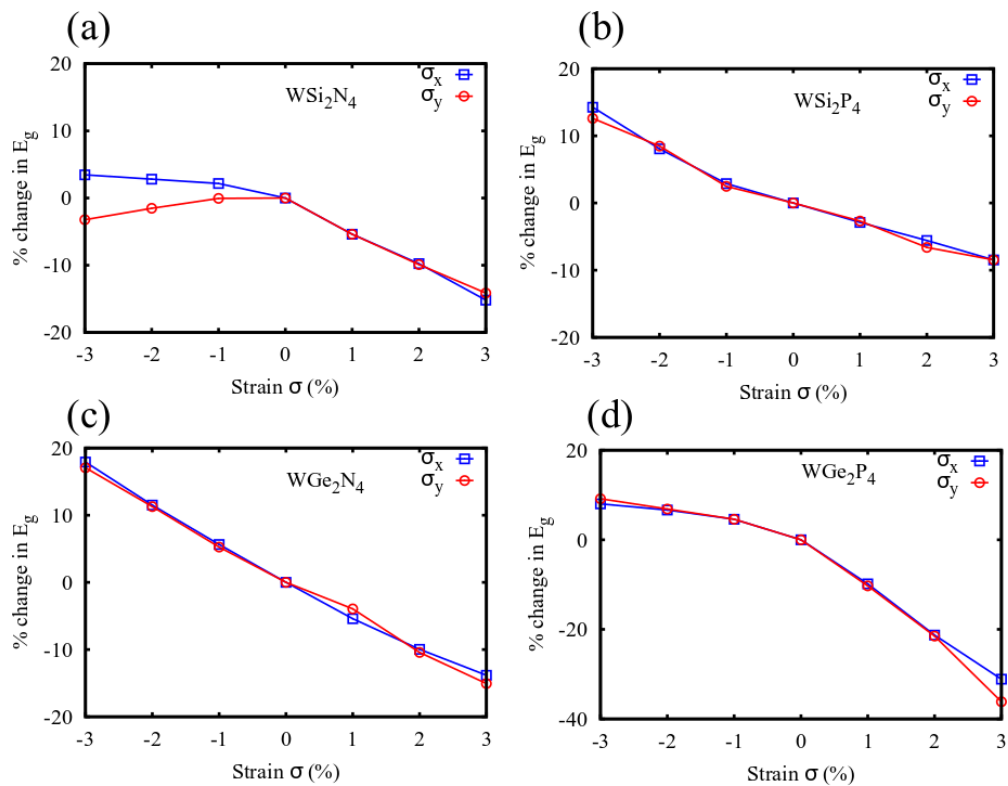**FIG. S13:** PDOS of (a) CrGe$_2$N$_4$ and (b) CrGe$_2$P$_4$ monolayers.

FIG. S14: (a)-(d) The % change in the electronic band gap of WA$_2$Z$_4$ monolayer as a function of the uniaxial strain along the x and the y axes.
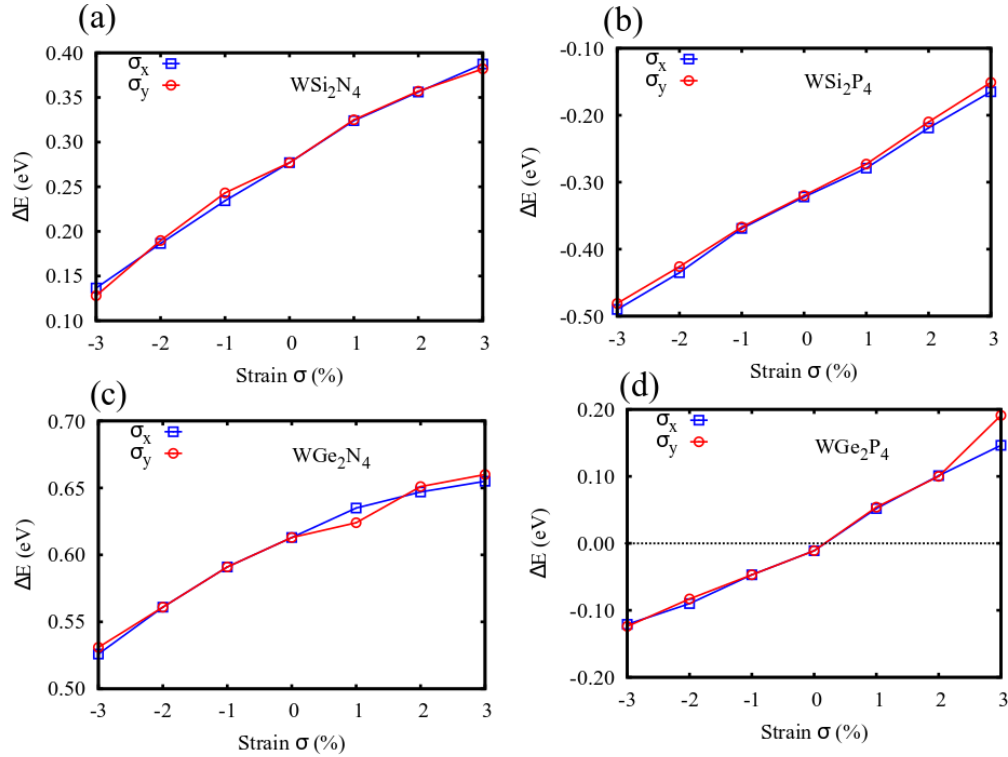
FIG. S15: (a)-(d) Change in the energy difference between the V_{Γ} and $V_{X'}$ points in WA_2Z_4 monolayer, defined as $\Delta E = E_{VBM}(\Gamma) - E_{VBM}(X')$. $\Delta E > 0$ implies that the VBM is located at the Γ point, and it also marks the indirect bandgap semiconductor regime since the CBM remains fixed at the X' point for the specified strain range. Thus, *only* WGe_2P_4 undergoes a direct to indirect bandgap transition, while the rest of the monolayers retain their zero strain characteristics.
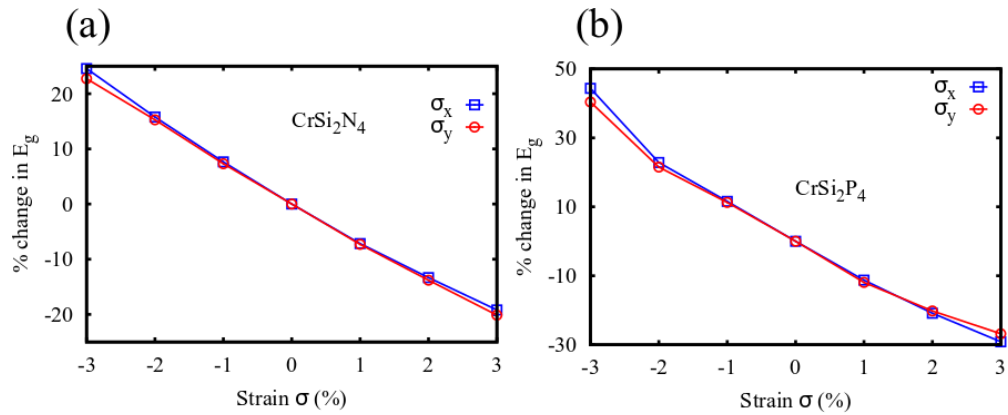

FIG. S16: The % change in the electronic band gap of (a) $CrSi_2N_4$ and (b) $CrSi_2P_4$ as a function of uniaxial strain along the x and y axes.
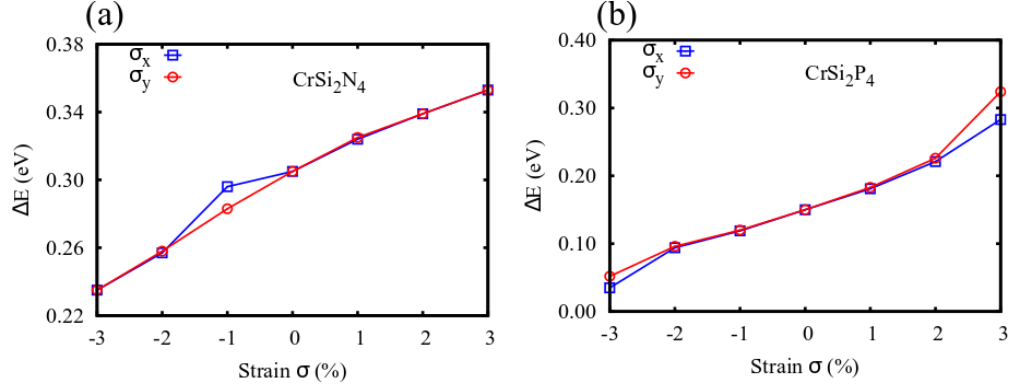
FIG. S17: Change in the energy difference between the V_Γ and $V_{X'}$ points in $CrSi_2N_4$ and $CrSi_2P_4$ monolayers, defined as $\Delta E = E_{VBM}(\Gamma) - E_{VBM}(X')$. $\Delta E > 0$ implies that the VBM is located at the Γ point, and it also marks the indirect bandgap semiconductor regime since the CBM remains fixed at the X' point for the specified strain range.
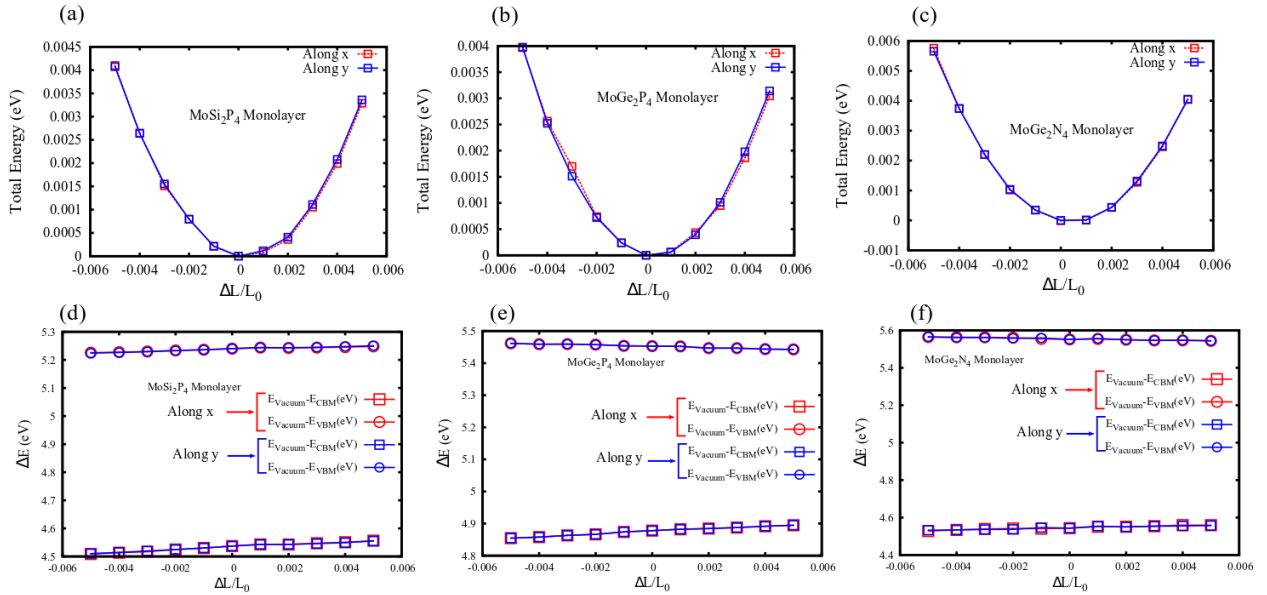

FIG. S18: (a)-(c) Energy-strain relationship along x and y directions in case of MoA_2Z_4 monolayers, except $MoSi_2N_4$. (d)-(f) Corresponding conduction band shift and valance band shift under uniaxial strain along x and y directions. The elastic constant is determined by parabolic fitting, while the DP constant is determined by linear fitting.
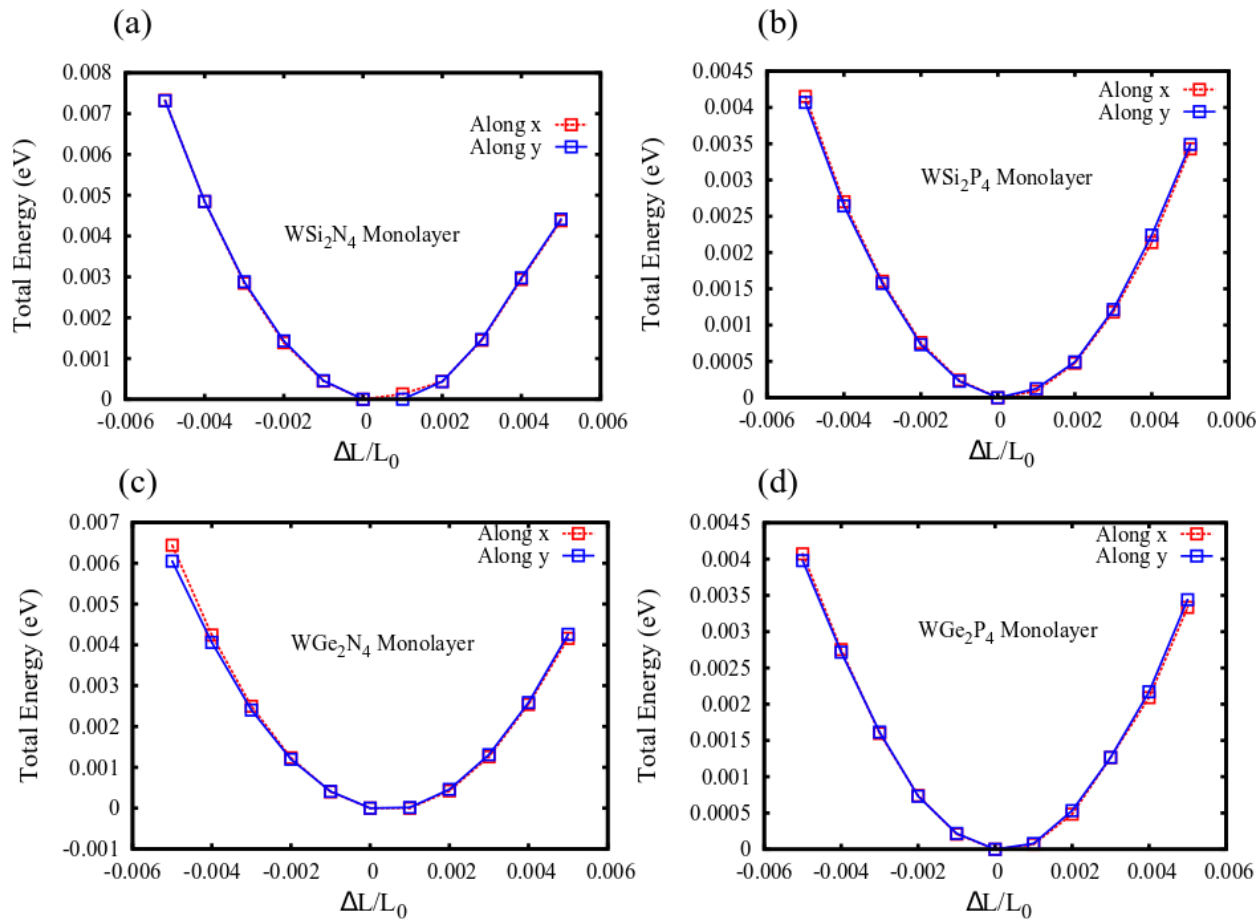
FIG. S19: Energy-strain relationship along x and y directions in case of WA_2Z_4 monolayer.
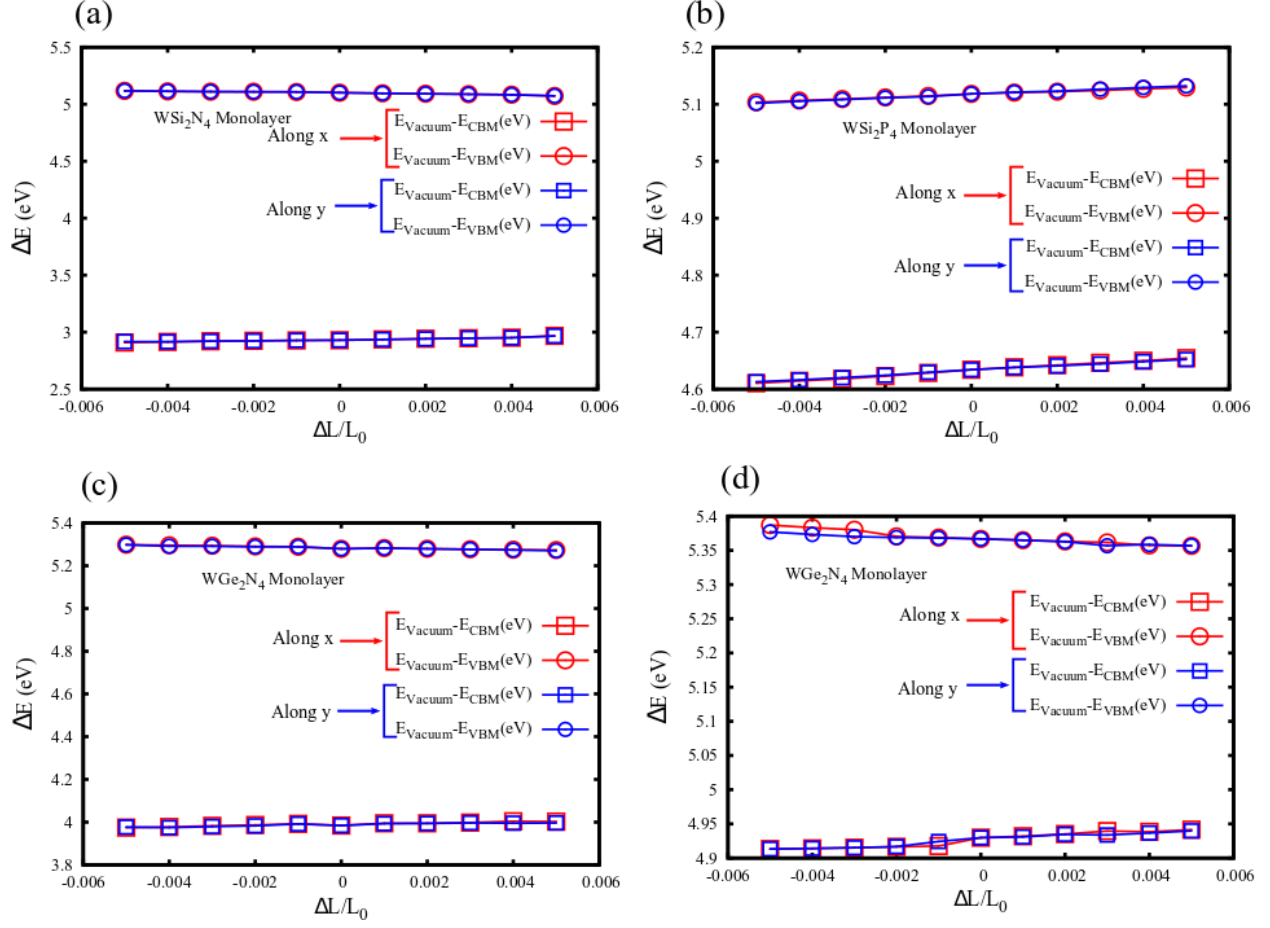
FIG. S20: Conduction band shift and valance band shift under uniaxial strain along x and y directions in case of WA$_2$Z$_4$ monolayers.
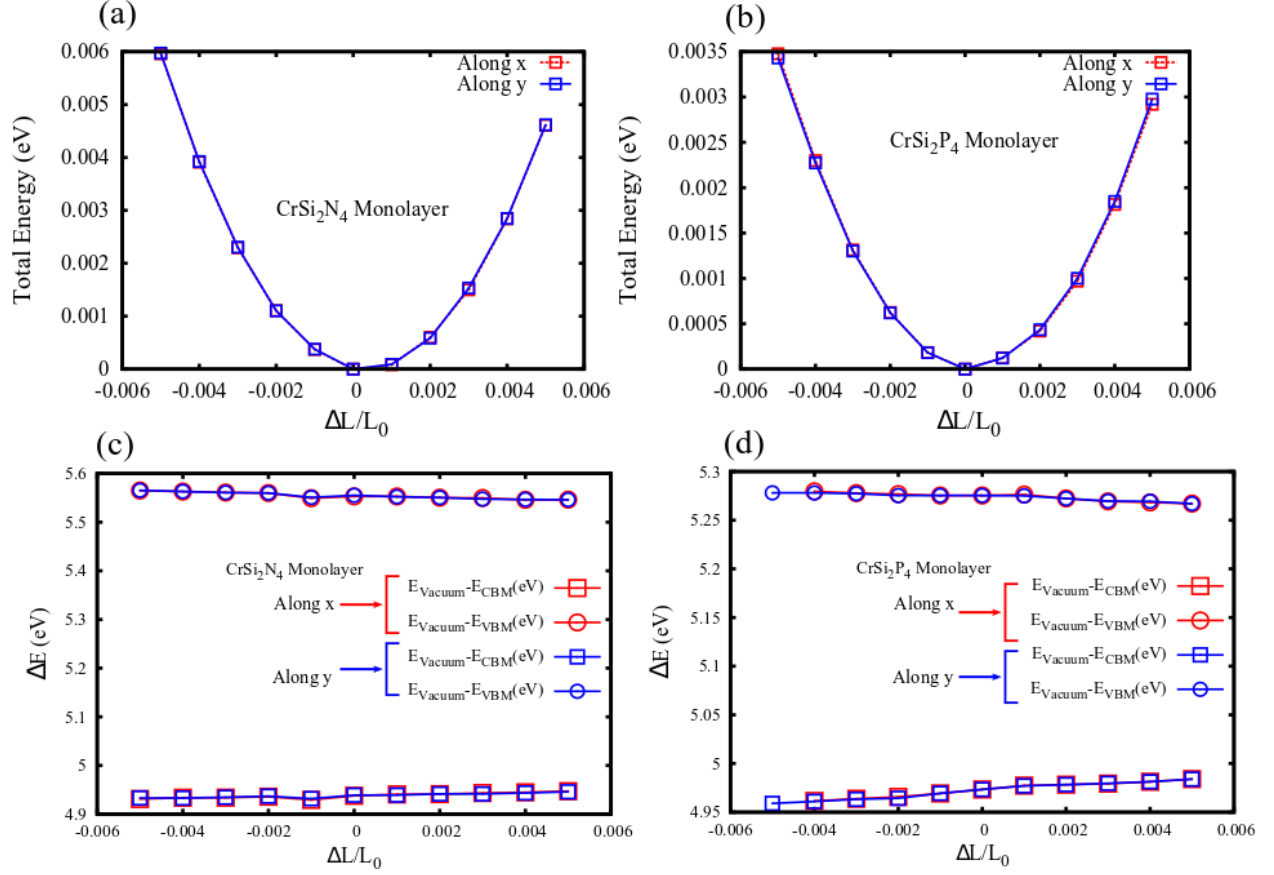
FIG. S21: (a)-(b) Energy-strain relationship along x and y directions. (c)-(d) Corresponding conduction band shift and valance band shift under uniaxial strain along x and y directions in case of $CrSi_2N_4$ and $CrSi_2P_4$ monolayers.

III.   MOBILITY CALCULATION

We have calculated mobility in MA_2Z_4 monolayers along the α ($\alpha = x/y$) direction as described in refs. [8, 9] and is given by

$$\mu_\alpha = \frac{2e\hbar^3 C_\alpha}{3k_B T m_\alpha^* \sqrt{m_\alpha^* m_\beta^*}(E_\alpha^i)^2} \ . \tag{S1}$$

$$\mu_\alpha = \frac{e\hbar^3 \left(\dfrac{5C_\alpha + 3C_\beta}{8}\right)}{k_B T m_\alpha^{1.5} m_\beta^{0.5} \left(\dfrac{9E_\alpha^2 + 7E_\alpha E_\beta + 4E_\beta^2}{20}\right)} \tag{S2}$$

and corresponding results are presented in Table S3.

A.   MOBILITY WITH SPIN-ORBIT COUPLING

To get more insight into the change in carriers' mobility due to spin-orbit coupling (SOC), we have calculated the effective mass of the charge carriers using the SOC band structure. We found that the change in the effective mass is ignorable in most cases. While in some monolayers, for example, WSi_2P_4 and WGe_2P_4, the effective mass corresponding to the VBM and CBM are reduced by a factor of about 1.4 when compared to the PBE value. This decrease in effective mass increases the carrier's mobility by a factor of about 2 (see Table S2).

[1] N. Jena, A. Rawat, R. Ahammed, M. K. Mohanta, A. De Sarkar, *et al.*, Emergence of high piezoelectricity along with robust electron mobility in janus structures in semiconducting group ivb dichalcogenide monolayers, Journal of Materials Chemistry A **6**, 24885 (2018).

[2] Y. K. Chung, J. Lee, W.-G. Lee, D. Sung, S. Chae, S. Oh, K. H. Choi, B. J. Kim, J.-Y. Choi, and J. Huh, Theoretical study of anisotropic carrier mobility for two-dimensional nb2se9 material, ACS omega **6**, 26782 (2021).

[3] M. Zhou, X. Chen, M. Li, and A. Du, Widely tunable and anisotropic charge carrier mobility in monolayer tin (ii) selenide using biaxial strain: a first-principles study, Journal of Materials Chemistry C **5**, 1247 (2017).

[4] T. Yu, Z. Zhao, Y. Sun, A. Bergara, J. Lin, S. Zhang, H. Xu, L. Zhang, G. Yang, and Y. Liu, Two-dimensional pc6 with direct band gap and anisotropic carrier mobility, Journal of the American Chemical Society **141**, 1599 (2019).

[5] Y. Zhou, L. Zhou, and J. He, 2d nb3sbr7 and ta3sbr7: Experimentally achievable janus photocatalysts with robust coexistence of strong optical absorption, intrinsic charge separation, and ultrahigh solar-to-hydrogen efficiency, ACS Applied Materials & Interfaces **14**, 1643 (2021).

[6] J. Zhao, X. Jin, H. Zeng, C. Yao, and G. Yan, Spin-valley coupling and valley splitting in the mosi2n4/crcl3 van der waals heterostructure, Applied Physics Letters **119**, 213101 (2021).

[7] X. Cai, Z. Zhang, Y. Zhu, L. Lin, W. Yu, Q. Wang, X. Yang, X. Jia, and Y. Jia, A two-dimensional mose 2/mosi 2 n 4 van der waals heterostructure with high carrier mobility and diversified regulation of its electronic properties, Journal of Materials Chemistry C **9**, 10073 (2021).

[8] J. Bardeen and W. Shockley, Deformation potentials and mobilities in non-polar crystals, Physical review **80**, 72 (1950).

[9] H. Lang, S. Zhang, and Z. Liu, Mobility anisotropy of two-dimensional semiconductors, Phys. Rev. B **94**, 235306 (2016).